Journal of Marine Systems 76 (2009) 496–510

Contents lists available at ScienceDirect

Journal of Marine Systems

journal homepage: www.elsevier.com/locate/jmarsys

Using satellite observations of ocean color to categorize the dispersal patterns of river-borne substances in the Gaoping (Kaoping) River, Shelf and Canyon system

Cheng-Chien Liu [a,*], Chih-Hua Chang [b], Ching-Gung Wen [b], Ching-Hsiang Huang [b], Jia-Jang Hung [c], James T. Liu [c]

[a] Department of Earth Sciences, Institute of Satellite Informatics and Earth Environment, Earth Dynamic System Research Center, Sustainable Environment Research Center, National Cheng Kung University, No 1, Ta-Hsueh Road, Tainan, 701 Taiwan ROC
[b] Department of Environmental Engineering, National Cheng Kung University, No 1, Ta-Hsueh Road, Tainan, 701 Taiwan ROC
[c] Institute of Marine Geology and Chemistry, National Sun Yat-sen University, Kaohsiung 80424, 701 Taiwan ROC

ARTICLE INFO

Article history:
Received 30 April 2007
Revised 2 November 2007
Accepted 3 November 2007
Available online 31 August 2008

Keywords:
Dispersal pattern
Chlorophyll-*a*
Suspended particles
Colored dissolved organic matter
Plume
Genetic algorithm
MODIS
QuikSCAT
Ocean color
Sea surface temperature
Sea surface wind
Gaoping (Kaoping) River

ABSTRACT

Mapping the water constituents from remotely sensed ocean color data enables a better understanding of the dispersal patterns of river-borne substances in the Gaoping (formerly spelled Kaoping) River, Shelf and Canyon (KPRSC) system. Based on twelve MODIS-Aqua images in the KPRSC region taken in 2005, we apply a newly developed GA-SA approach to derive maps of chlorophyll-*a* concentration (*Chl-a*), colored dissolved organic matter (CDOM) and non-algal particle/detritus/mineral (NAP). The results demonstrated that the different characteristics of *Chl-a*, CDOM and NAP make them ideal tracers for observing large-scale dispersal patterns. With ancillary information of averaged daily precipitation, the daily wind field obtained from QuikSCAT (Quick Scatterometer), and the 8-day composite of the temperature field obtained from MODIS-Aqua, we categorized the surface dispersal patterns as coastal, northwestward and frontal patterns. Also, for the first time, we observed a sudden increase of biomass on a large scale from a pair of ocean color images taken over only a 2-day interval. Another remarkable feature is the interaction between the southeastward flow and the intrusion of the Kuroshio Branch, resulting in complicated patterns with various scales of vortex structures and current fronts. The observed features could be used for model validation of the flow field of the KPRSC system.

1. Introduction

The major goals of the FATES-KP (Fate of Terrestrial Substances in Gaoping (Kaoping) Submarine) project are to identify, characterize, and quantify the generation of fluvial substances, their movement and change along the fluvial and estuarine conduit, the pattern of dispersal and transformation in the Gaoping (Formerly spelled Kaoping) River, Shelf and Canyon (KPRSC), and the sources, pattern and fluxes and deposition in the receiving submarine canyon. In recent findings, Liu and Lin (2004) showed that the river plume and coastal wind field largely control the delivery of terrestrial fine-grained sediment to the canyon. Hung et al. (2004) reported that significant carbon and nutrient productions related to the typhoon and monsoon climate are likely derived from anthropogenic sources in the river basin. Regular cruises have been conducted by the FATES project since 2000. However, to gain a better understanding of the role that the KPRSC plays in determining the dispersion of river-borne materials, it is necessary to expand from point measurements to spatial coverage over the entire region of the KPRSC.

* Corresponding author. Tel.: +886 6 2757575x65422; fax: +886 6 2740285.
E-mail address: ccliu88@mail.ncku.edu.tw (C.-C. Liu).

0924-7963/$ – see front matter © 2008 Elsevier B.V. All rights reserved.
doi:10.1016/j.jmarsys.2007.11.013

Satellite remote sensing provides long-term, synoptic observations of the earth's surface from space, and satellite sea surface temperature (SST) and sea surface wind (SSW) have been widely used in oceanography. To study the dispersion of river-borne materials, it is necessary to determine the distributions of various water constituents in order to trace the surficial fluvial flux. Mapping the water constituents in the coastal zone was one of the original objectives of the first space-borne ocean color mission in 1978, namely the Coastal Zone Color Scanner (CZCS) (Barale and Schlittenhardt, 1993). Although the pigment concentrations in the open oceans turned out to be the only reliable product that could be derived from the CZCS mission, the original objective is still a goal that numerous follow-up missions are attempting to attain (Hooker et al., 1992). For instance, the successful deployment of two MODerate resolution Imaging Spectroradiometers (MODIS) onboard TERRA (December 1999) and AQUA (May 2002) have largely increased the spectral resolutions in the visible/near-infrared range from 5 bands with a bandwidth of 20 nm (CZCS) to 9 bands with a bandwidth of 10 nm, and the radiometric resolutions from 8-bit

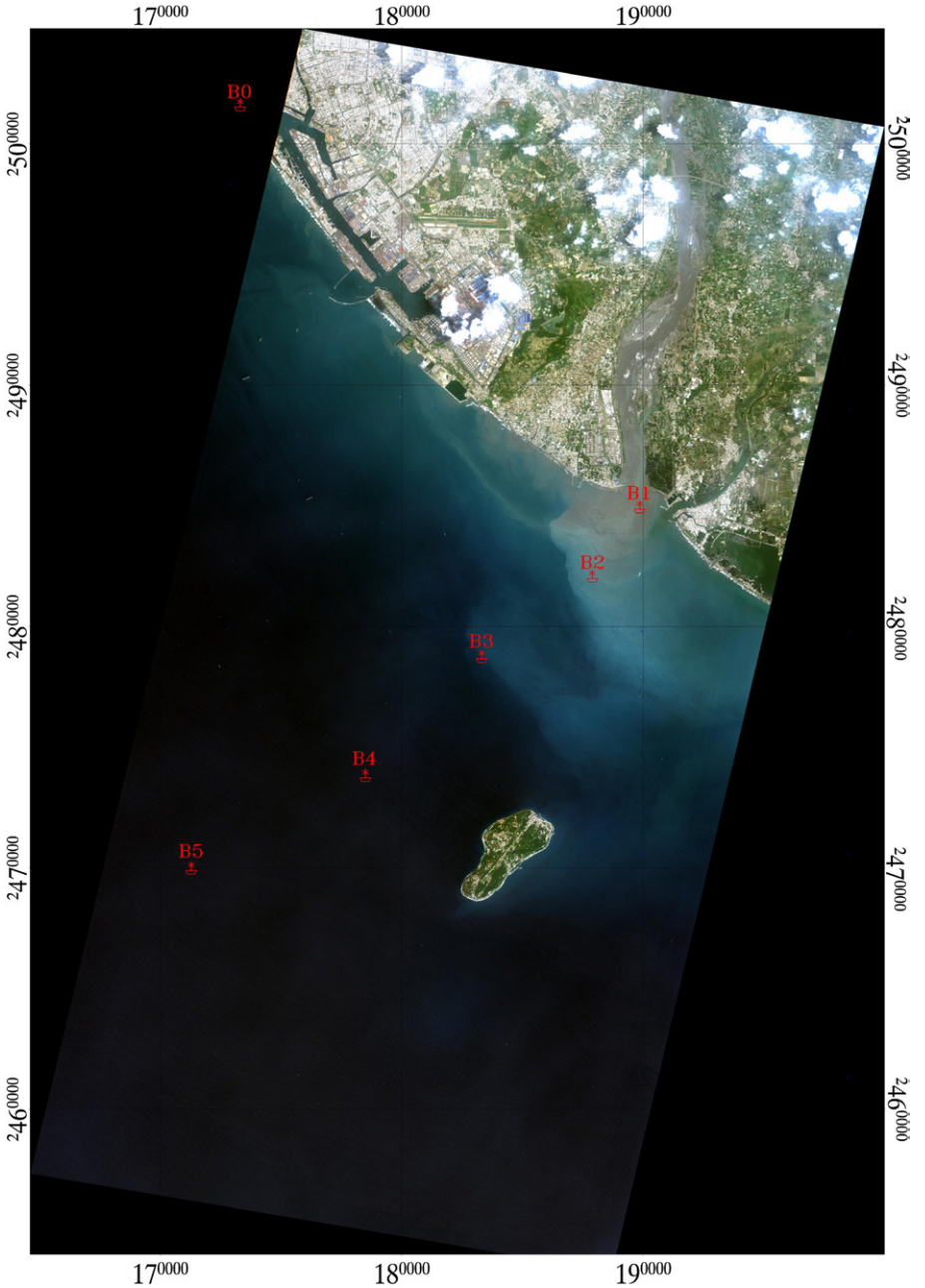

Fig. 1. Illustration of the spatial variation in the KPRSC region. The true-color multi-spectral image with 8-m resolution was taken by the FORMOSAT-2 on 10 August 2005. Regular cruises were conducted by the FATES project to collect and analyze the water samples from station B1 to B5, as denoted in red.

(CZCS) to 12-bit. The International Ocean Color Coordinate Group (IOCCG) has also compiled two comprehensive datasets comprised of synthetic data and *in-situ* measurements to provide an objective evaluation of various retrieval algorithms (Lee, 2006). The recent progress of integrating the semi-analytical (SA) algorithm and the genetic algorithm (GA) has demonstrated that the water constituents, such as chlorophyll-*a* concentration (*Chl-a*), colored dissolved organic matter (CDOM) and non-algal particle/detritus/mineral (NAP), can be routinely derived from ocean color remote sensing (Chang et al., 2007). This motivates us to apply the GA-SA approach to process the MODIS images for regional maps of *Chl-a*, CDOM and NAP in the KPRSC system, with the intention of gaining a better understanding of the dispersal patterns of river-borne substances.

After screening a total of 290 scenes taken by MODIS-Aqua of the KPRSC region in 2005, twelve images of low cloud-coverage were processed by the GA-SA approach to generate the maps of *Chl-a*, CDOM and NAP. Water samples and the spectrum of above-surface remote sensing reflectance ($R_{rs}(\lambda)$) were collected around the overpass of MODIS-Aqua on November 23, 2005 to verify the results of our GA-SA derived *Chl-a* and CDOM. After validation, twelve maps of *Chl-a*, CDOM and NAP were used to study the dispersal patterns of river-borne substances in the KPRSC system. Ancillary information of averaged daily precipitation, the daily wind field obtained from QuikSCAT (Quick Scatterometer), and the 8-day composite of sea surface temperature obtained from MODIS-Aqua were used to describe the environmental conditions. The surface dispersal patterns were categorized, and the possible mechanisms are discussed.

2. Data

2.1. Study area

The study area encompasses the southwestern tip of the island of Taiwan and the northeastern corner of the South China Sea basin. The Gaoping River (KPR) is the largest river in Taiwan in terms of the basin area and river length. Because of the geology, topography, climate, and human activities in the river basin, both physical weathering and chemical weathering rates are very high (Hung et al., 2004). Recent studies show that sediment yield from the KPR watershed (5.9 kg/m^2/yr, Hung and Hung, 2003) is much higher than the mean value (3 kg/m^2/yr, Milliman and Syvitski, 1992) of global mountainous rivers. High rates of sediment loading from the KPR are usually concentrated with considerable spatial and temporal variations in a small fluvial conduit (approximately 6.4 km^2). This is illustrated in the true-color multi-spectral high spatial resolution (8 m) image of the study area taken by the FORMOSAT-2 on 10 August 2005 (Fig. 1). In order to gain a better understanding of the crucial phenomena, such as the exchange of water mass and suspended particles (Liu et al., 2006, 2002), the FATES project conducts regular cruises onboard the R/V Ocean Researcher III to collect and analyze the water samples at five stations spanning from the river mouth to the canyon (as denoted from B1 to B5 in Fig. 1).

2.2. Ground observations

For most of the river systems, the main source of sediments delivered to the ocean is through the erosion of the watershed

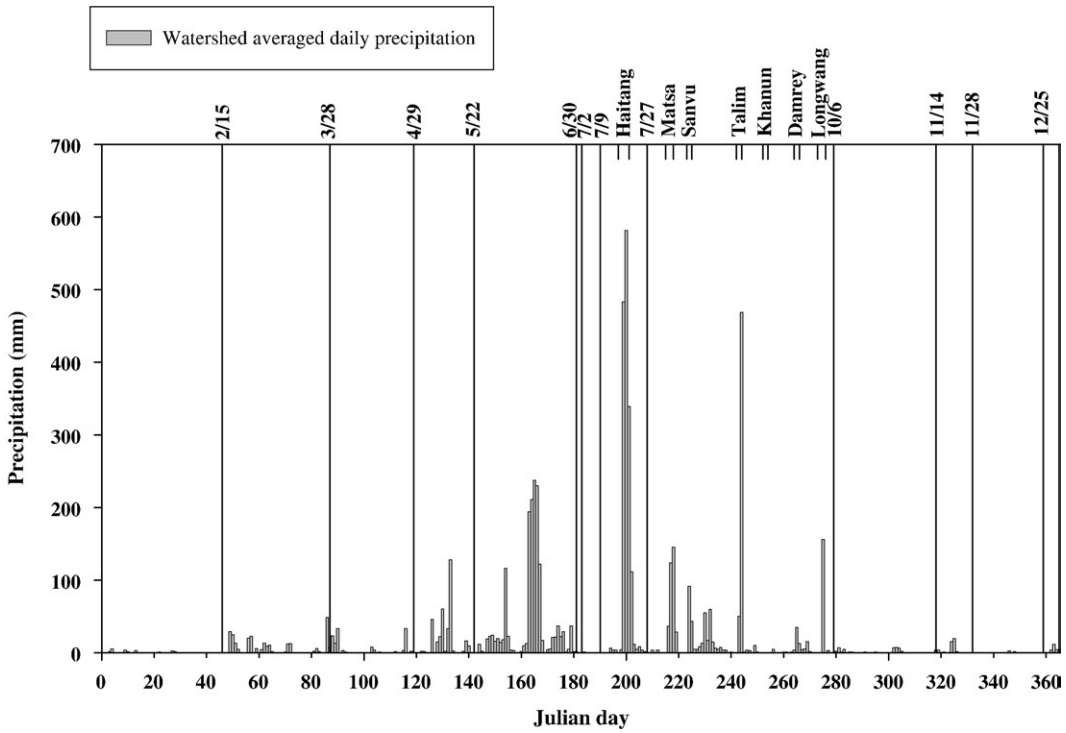

Fig. 2. The averaged daily precipitation in the watershed of the KPR by applying the Thiessen polygons method to analyze the data collected by 17 rain-gauge stations in the watershed (Fig. 3).

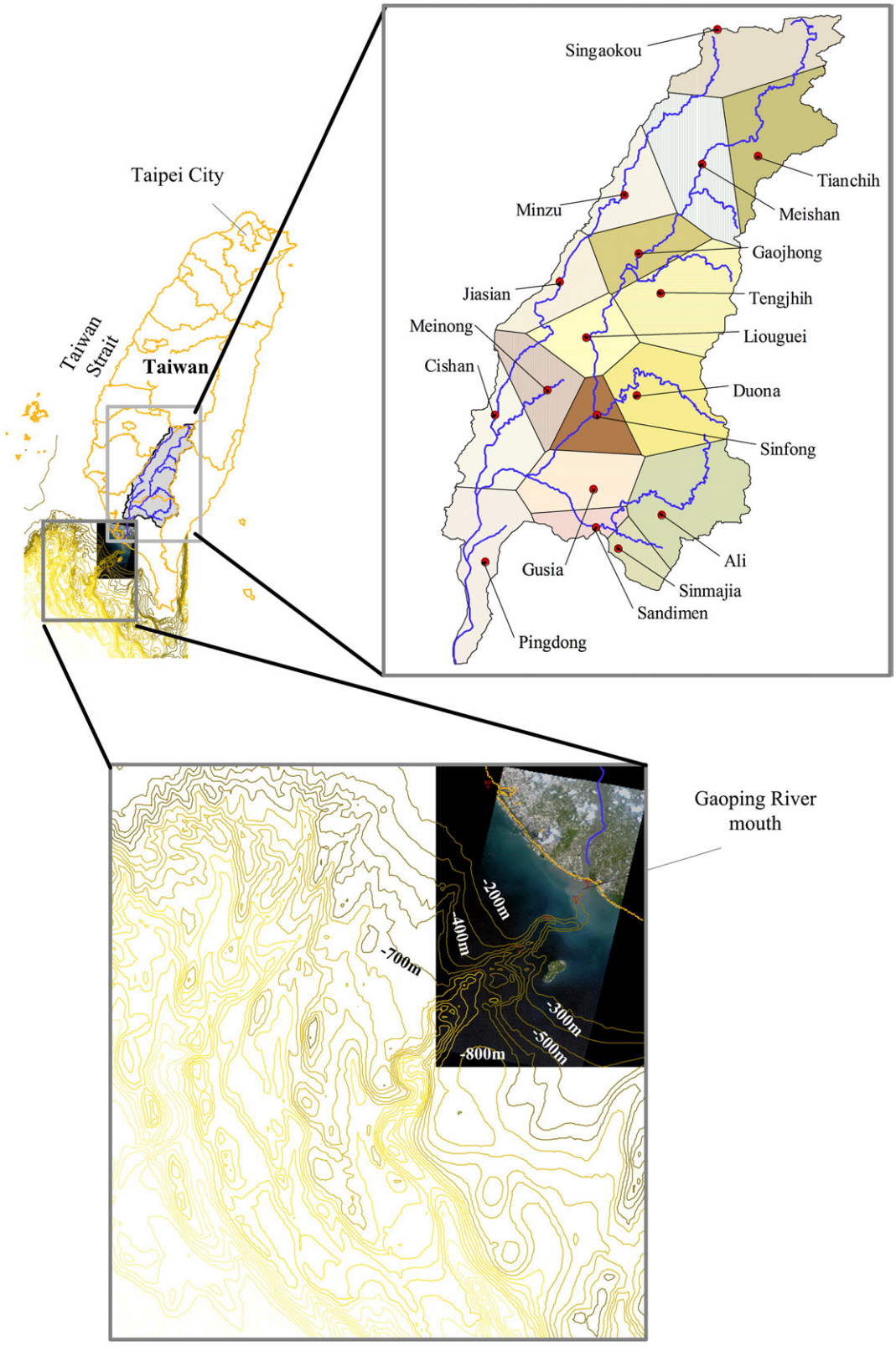

Fig. 3. The geographical locations and the sub-basin areas of 17 rain-gauge stations in the watershed of the KPR.

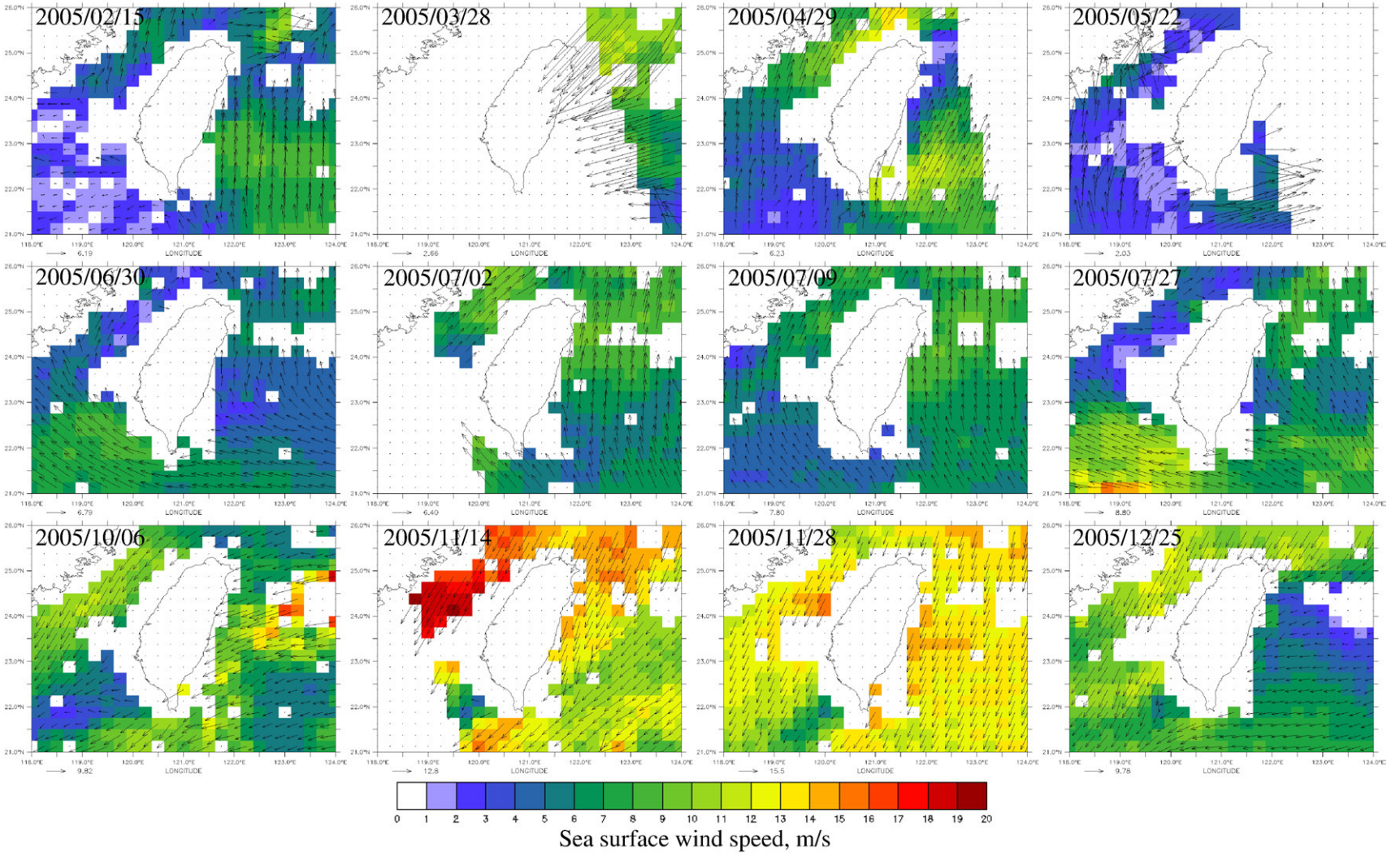

Fig. 4. Maps of sea surface wind derived by QuikSCAT images with a 0.25-degree spatial resolution and a 1-day temporal resolution.

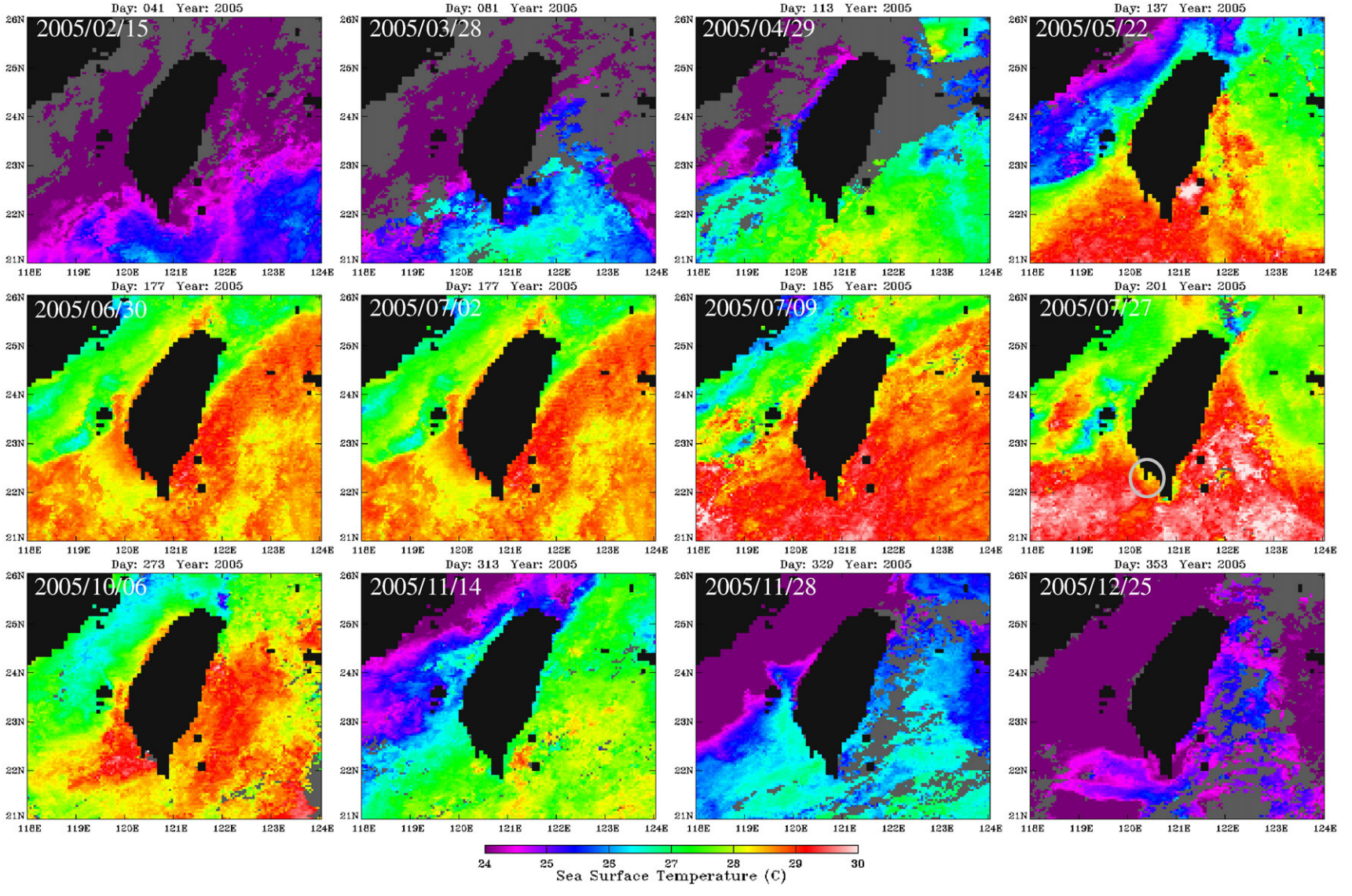

Fig. 5. Maps of sea surface temperature derived by MODIS-Aqua images with a 4-km spatial resolution and an 8-day temporal resolution.

substrates during major rainfall events. The crucial information of averaged daily precipitation in the watershed of KPR is obtained (Fig. 2) by applying the Thiessen polygons method to analyze the data collected in 17 rain-gauge stations in the watershed (Fig. 3). The vertical lines in Fig. 2 indicate twelve dates of low-cloud-coverage images taken by MODIS-Aqua in 2005. The typhoon events are denoted in Fig. 2 for reference.

2.3. Satellite observations of SSW and SST

The QuikSCAT mission, successfully launched in 1999, has been providing wind-speed measurements from 3 to 20 m/s with an accuracy of 2 m/s, and wind-direction measurements with an accuracy of 20°. The Advanced Very High Resolution Radiometer (AVHRR) and MODIS-Aqua have also been providing the SST product. To enable the users, NASA has provided a tool, POET, developed by the Ocean Earth Science Information Partner (ESIP), to easily subset, plot, and view various satellite data products. We employed this tool to generate the maps of SSW from the QuikSCAT with a 0.25-degree spatial resolution and a 1-day temporal resolution (Fig. 4), and the maps of SST from the MODIS-Aqua with a 4-km spatial resolution and an 8-day temporal resolution (Fig. 5). Note that a total of twelve dates are selected, which correspond to the color images in the KPRSC region taken by MODIS-Aqua in 2005.

The grided QuikSCAT SSW gives a smoothed wind field. Although the QuikSCAT data is restricted in the coastal region (masked as gray squares in Fig. 4), we may reasonably infer the wind field in the KPRSC from the overall pattern. The following is a brief description of the wind field in the KPRSC as seen in Fig. 4. Generally speaking, mild easterly and north-easterly wind prevails in early spring (2/15 and 3/28), but it reverses to a southerly and southwesterly wind in late spring and early summer (4/29 and 5/22). A steady and moderate southeasterly wind prevails during the entire summer time (6/30, 7/2, 7/9 and 7/27), and reverses to a north-easterly wind in autumn and becomes stronger in the winter (10/6, 11/14, 11/28 and 12/25). The seasonal cycle follows the East Asia monsoon pattern.

The SST product used in this study is for consistency from MODIS-Aqua rather than AVHRR, mainly because we are primarily interested in the ocean color data acquired by MODIS-Aqua. Also, we select the 8-day composite, as the daily SST image is often masked by cloud cover. The SST generally shows the seasonal progression of the Kuroshio warm front. The regions of water with higher temperatures gradually stretch from southeast to northwest as the weather becomes warmer. Likewise, the boundary retreats from northwest to southeast as the weather becomes colder. Both the satellite observations of SSW and SST provide the environmental conditions in the KPRSC.

2.4. Satellite observations of ocean color

All MODIS-Aqua images of the KPRSC region taken in 2005 were downloaded from the Ocean Color web site (http://oceancolor.gsfc.nasa.gov/). The level-2 local area coverage (LAC) data was preprocessed by the SeaWiFS Data Analysis System (SeaDAS) to generate the georeferenced image of the normalized water-leaving radiance for each spectral band, $\hat{L}_W(\lambda)$. $R_{rs}(\lambda)$ is obtained by dividing $\hat{L}_W(\lambda)$ with the spectral values of the extraterrestrial solar irradiance $F_0(\lambda)$ (http://oceancolor.gsfc.nasa.gov/DOCS/RSR_tables.html). The maps of *Chl-a*, CDOM and NAP were generated by following the procedures described in Chang et al. (2007). Table 1 shows the dynamic ranges of 9 decision variables in the bio-optical model. Table 2 gives values of control parameters used in GA. All processing is conducted on a personal computer equipped with a Pentium 2.4 GHz. For one scene with 4060 pixels, it takes about 10 min to download and preprocess the MODIS data using SeaDAS, and approximately 3 h to generate the maps of *Chl-a*, CDOM and NAP.

Table 1
The dynamic ranges of nine decision variables in bio-optical model

Decision variable	a_{ph} (440)	R_g	R_d	S_d	S_g	R_{bph}	R_{bd}	Y_{ph}	Y_d
Lower bound	0.008	0.3	0.1	0.01	0.007	0.005	0.01	−0.1	−0.2
Upper bound	0.5	6.0	0.6	0.02	0.015	0.15	0.4	2.0	2.2

Table 2
Values of control parameters used in GA

Number of generations	Number of individuals in a generation	Probability of crossover	Probability of mutation
500	50	0.6	0.05

The GA-SA approach has been carefully validated using the two comprehensive IOCCG datasets, which are comprised of synthetic data and *in-situ* measurements (Lee, 2006). The linear percentage errors between derived and measured a_{ph} values are less than 40% for the synthetic dataset and less than 86% for the *in-situ* dataset (details referred to Tables 3 and 4 in Chang et al., 2007). Compared to the other methods, the GA-SA approach provides better retrievals for both the inherent optical properties and various water constituents. Since the synthetic dataset comprises a wide range of parameters characterizing the global ocean (Case 1 waters), and most of the *in-situ* data come from locations that are relatively close to the coast (some are Case 2 waters) (Lee, 2003), the application of the GA-SA approach to the KPRSC region should give about the same level of accuracy.

To make rigorous validation of the GA-SA method will require a complete set of *in-situ* measurements that covers both the inherent and apparent optical properties as well as the detailed analysis of all constituents in the water samples. Despite the fact that these measurements and analyses are not included in the regular FATES cruises, we attempt to use the data collected during the cruise ORIII-CR1115 at station B5 around the overpass of MODIS-Aqua on November 23, 2005 to verify the results of the GA-SA derived *Chl-a* and CDOM (Table 3). $R_{rs}(\lambda)$ was determined by correcting for the surface-reflected skylight and solar glint from the above-surface total reflectance, which are measured from a hyper-spectral

Table 3
Indirect validation of the GA-SA derived *Chl-a* and CDOM (a_g (443))

	a_g (443) (m^{-1})	*Chl-a* (mg m^{-3})
Measurement	0.020	0.110
GA-SA derived	0.017	0.117
Error (%)	−15.0	6.3

The water samples were collected at station B5 at around 12:30 pm on 23 November 2005 during the cruise ORIII-CR1115. The overpass of MODIS-Aqua was made on the same day at around 1:30 pm local time.

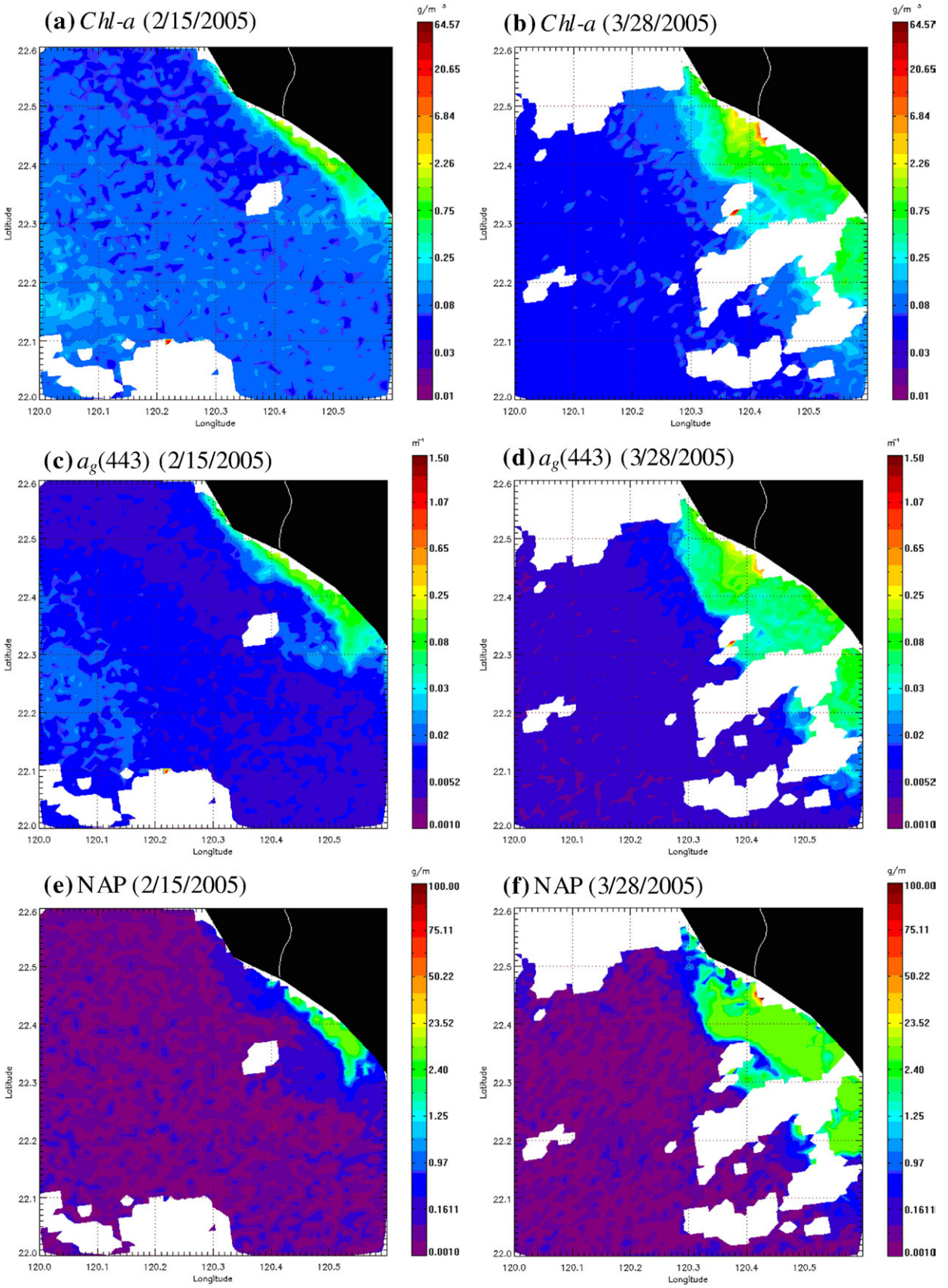

Fig. 6. Maps of *Chl-a*, a_g (443) and NAP derived from the MODIS-Aqua images of the KPRSC region taken in the late winter (2/15/2005) and early spring (3/28/2005).

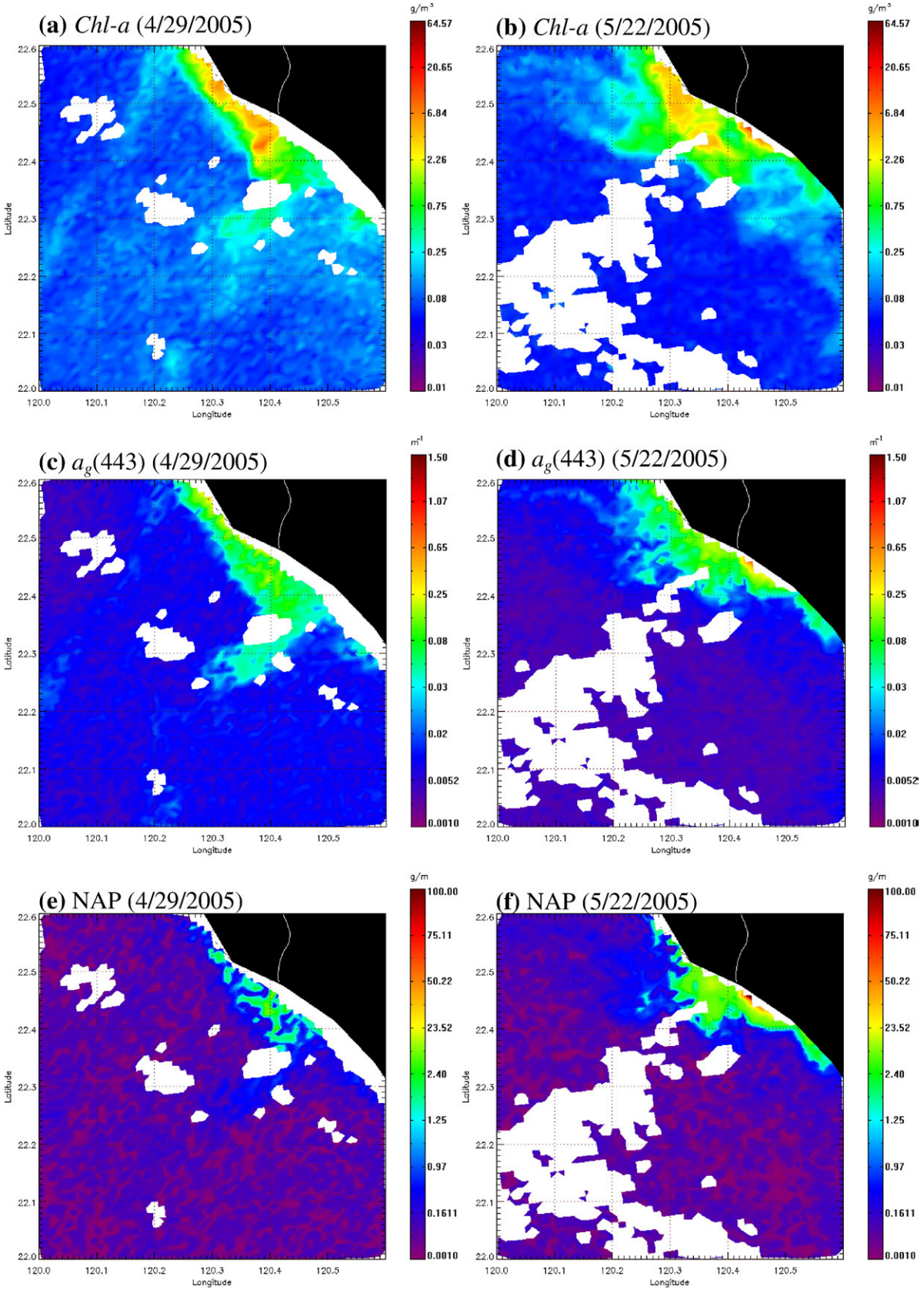

Fig. 7. Maps of *Chl-a*, a_g (443) and NAP derived from the MODIS-Aqua images of the KPRSC region taken in late spring (4/29/2005) and the "plum rain" season (5/22/2005).

handheld radiometer (Ocean Optics USB-2000). The details of the method are given in Lee et al. (1998) and Mobley (1999). The concentration of *Chl-a* is determined via a fluorometer (Turner Designs, model 10-AU) following the non-acidification technique (Welschmeyer, 1994). The spectral absorption coefficients of particles a_d, dissolved material a_g and phytoplankton a_{ph} for each water sample is determined by the spectro-photometric method following the procedures described by Mitchell et al. (2003). Details of the instruments and data processing of all stations are described in Huang (2006) and Yung (2006). Note that in the following discussion we employ the absorption coefficient of CDOM at 443 nm a_g (443) to represent the amount of CDOM. The *in-situ* measurement was made about 1 h before the MODIS-Aqua image was taken. The *in-situ* measurement is also a point measurement which is not necessarily equal to the average signal taken within 1 pixel (1 km×1 km) on the satellite image. Nevertheless, under the assumption that both the spatial and temporal variations were not significant at station B5 around the overpass of MODIS-Aqua, the comparable values shown in Table 3 provide an indirect way to validate the results of our GA-SA derived *Chl-a* and CDOM.

3. Results and discussion

The *Chl-a* from the satellite image of ocean color has been widely used as a tracer for studying plume dispersal patterns, e.g., Toner et al. (2003). However, an increase of *Chl-a* might exhibit a delay of a few days after an extra supply of nutrients are transported to the study area. Therefore, *Chl-a* might not reflect the actual timing and range of the change of water property. Furthermore, the general approach in deriving *Chl-a* from a satellite ocean color image cannot isolate contributions from the other constituents, such as CDOM or NAP. By contrast, CDOM is a better tracer for studying the dispersal pattern because it is completely dissolved in the water. If the supply is greater than the utilization rate, CDOM will spread more broadly than *Chl-a*. NAP refers to any non-algal particle, detritus or mineral. It is highly correlated to the sediment loading near the river mouth. Therefore, NAP can be used as a tracer for terrestrial materials. The GA-SA approach allows us to clarify the contributions to $R_{rs}(\lambda)$ from *Chl-a*, NAP and CDOM. Their different characteristics assist us in gaining a better understanding of the dispersal patterns of river-borne substances in the KPRSC system.

3.1. Coastal pattern

Figs. 6 and 7 show the maps of *Chl-a*, CDOM and NAP in the spring and early summer. Because the wind direction varies nearly everyday and the wind speed is comparatively low, the dispersal pattern during this period of time is mainly due to the influence of tide and current. In the case of a weak plume event (2/15 and 4/29) with low precipitation (Fig. 2), the river-borne material was stretched to a thin strip and transported as far as a few tens of kilometers away from the river mouth. In the case of a stronger plume event (3/28 and 5/22) with a higher precipitation rate (Fig. 2), the plume still followed the same pattern but expanded seaward much further. Note that there was no significant difference among the patterns of *Chl-a*, CDOM or NAP observed on the same day. This suggests that the NAP component was well-suspended and its distribution was approximately consistent with the river effluent. The same approximate ratio between *Chl-a* and CDOM across the entire region also suggests that the utilization of CDOM and the population of phytoplankton have reached a steady state. The observed patterns of *Chl-a*, CDOM or NAP, however, are rather different on 5/22. The annual rainy (*Meiyu*) season in May and June usually brings a lot of precipitation to Taiwan (Fig. 2). A considerable amount of river-borne materials appeared in the first available image taken during the rainy season (5/22). Note that NAP is unevenly distributed and concentrated in a small core near the river mouth. This suggests a strong plume event and that most of the NAP might be larger and heavier river-borne particles that cannot suspend for very long. The difference in the *Chl-a* and NAP pattern also supports this argument.

3.2. Northwestward pattern

During the summer, the wind is southeasterly and mild (Fig. 4) and leads to a continuously northwestward transport of the river-borne materials. An event of a phytoplankton bloom is revealed by a pair of images taken over a 2-day interval (Fig. 8). Although the orbit and the swath of MODIS-Aqua are designed to achieve a repeat rate as high as 1 or 2 days, it is rare to obtain repeat images in the KPRSC region in less than one week intervals due to cloud-coverage. Fortunately, there were two successive images taken on 6/30/2005 and 7/2/2005. Fig. 8 shows the dramatic increase of *Chl-a* in 2 days; however, the CDOM and NAP remain at about the same level. The cause for the bloom, though, is not obvious.

The largest rainfall event in 2005 was brought on by Typhoon Haitang (Fig. 2). Two images were taken before (7/9/2005) and after (7/27/2005) this event, and are shown in Fig. 9. The largest discharge event came after the largest rainfall. The large-scale discharge during the storm or heavy rainfall is almost always blocked by clouds, and hence, no information can be retrieved from the ocean color image. Fig. 9 gives a rare case of the large discharge event over the canyon. The meander pattern shown of *Chl-a* is remarkably consistent with the bathymetry of the canyon. This feature, however, is not shown on CDOM or NAP. Since their coverage also indicates the transport range of river-borne materials, there should be another source of nutrient to support such a large-scale bloom of phytoplankton. As revealed by the SST image taken after Typhoon Haitang (7/27), a large patch of cold water is also observed in our study area (as circled in Fig. 5). This suggests an upwelling event, pumped by the passage of the typhoon, is also an important mechanism for boosting the short-term productivity in the river–sea system.

3.3. Frontal pattern

Wind direction turns north-easterly in the fall and is strengthened in the winter (Fig. 4). Since Taiwan and its adjacent regions are all covered by the strengthened north-easterly wind during the winter, the current in the Taiwan Strait basically flows from the north to the south. The transport is expected to be southeastward as in the spring. However, the region of water with higher temperatures is still over the Taiwan Strait (Fig. 5), and the precipitation is low in

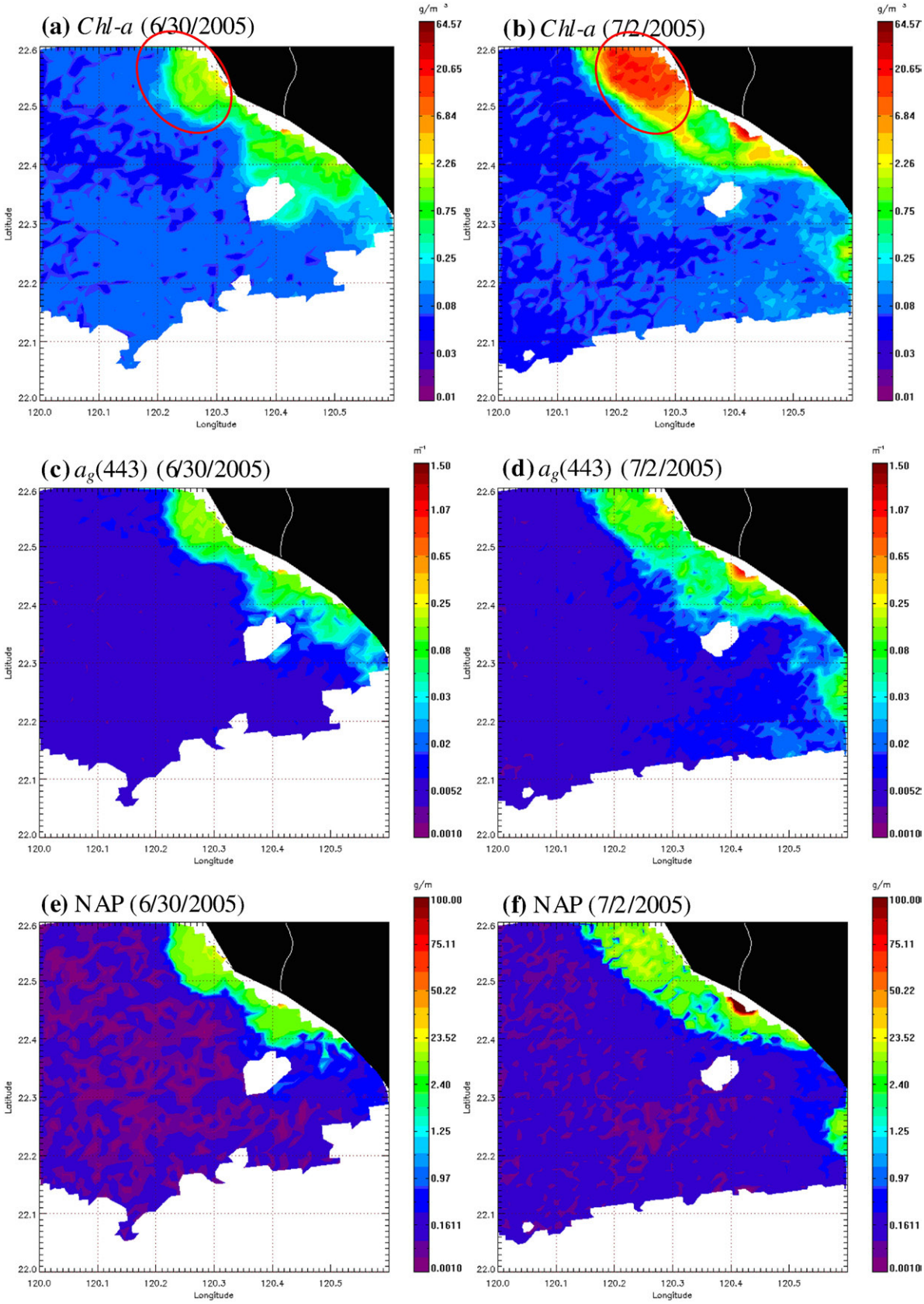

Fig. 8. Maps of *Chl-a*, a_g (443) and NAP derived from the MODIS-Aqua images of the KPRSC region taken over a 2-day interval (6/30/2005, 7/2/2005).

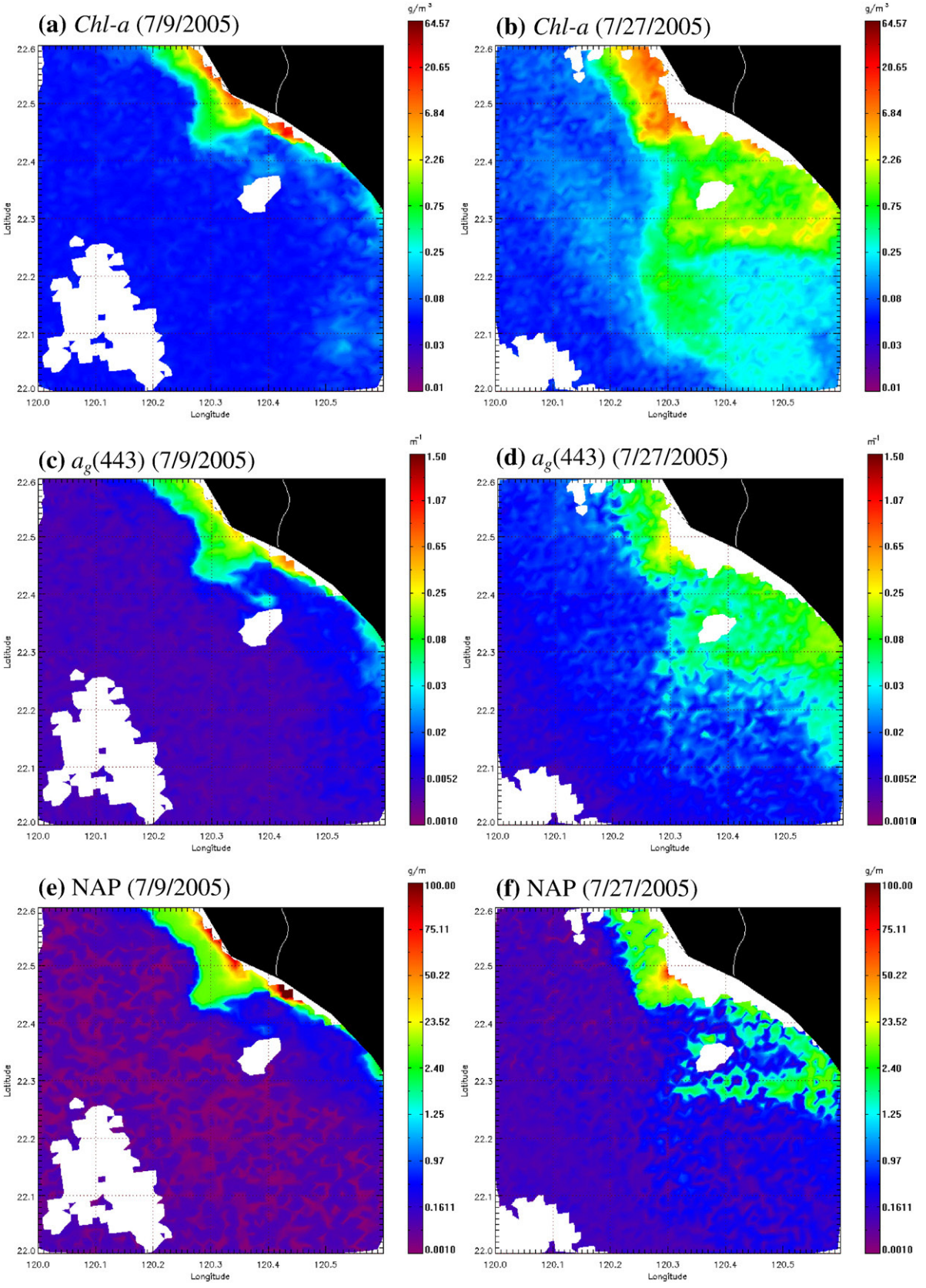

Fig. 9. Maps of *Chl-a*, a_g (443) and NAP derived from the MODIS-Aqua images of the KPRSC region taken right before (7/9/2005) and after the Haitang typhoon (7/27/2005).

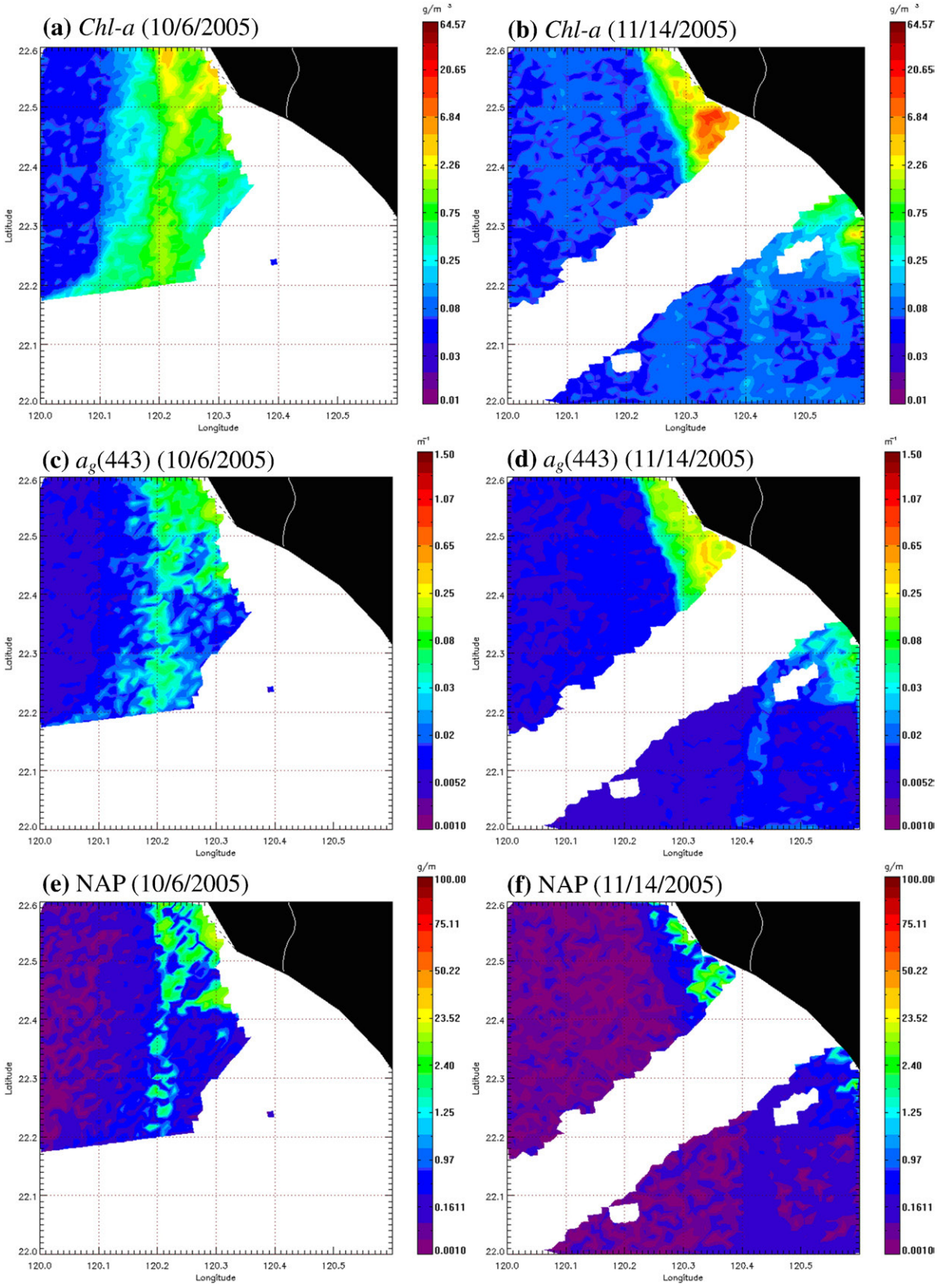

Fig. 10. Maps of *Chl-a*, a_g (443) and NAP derived from the MODIS-Aqua images of the KPRSC region that show the front (10/6/2005) and the small vortex structure (11/14/2005).

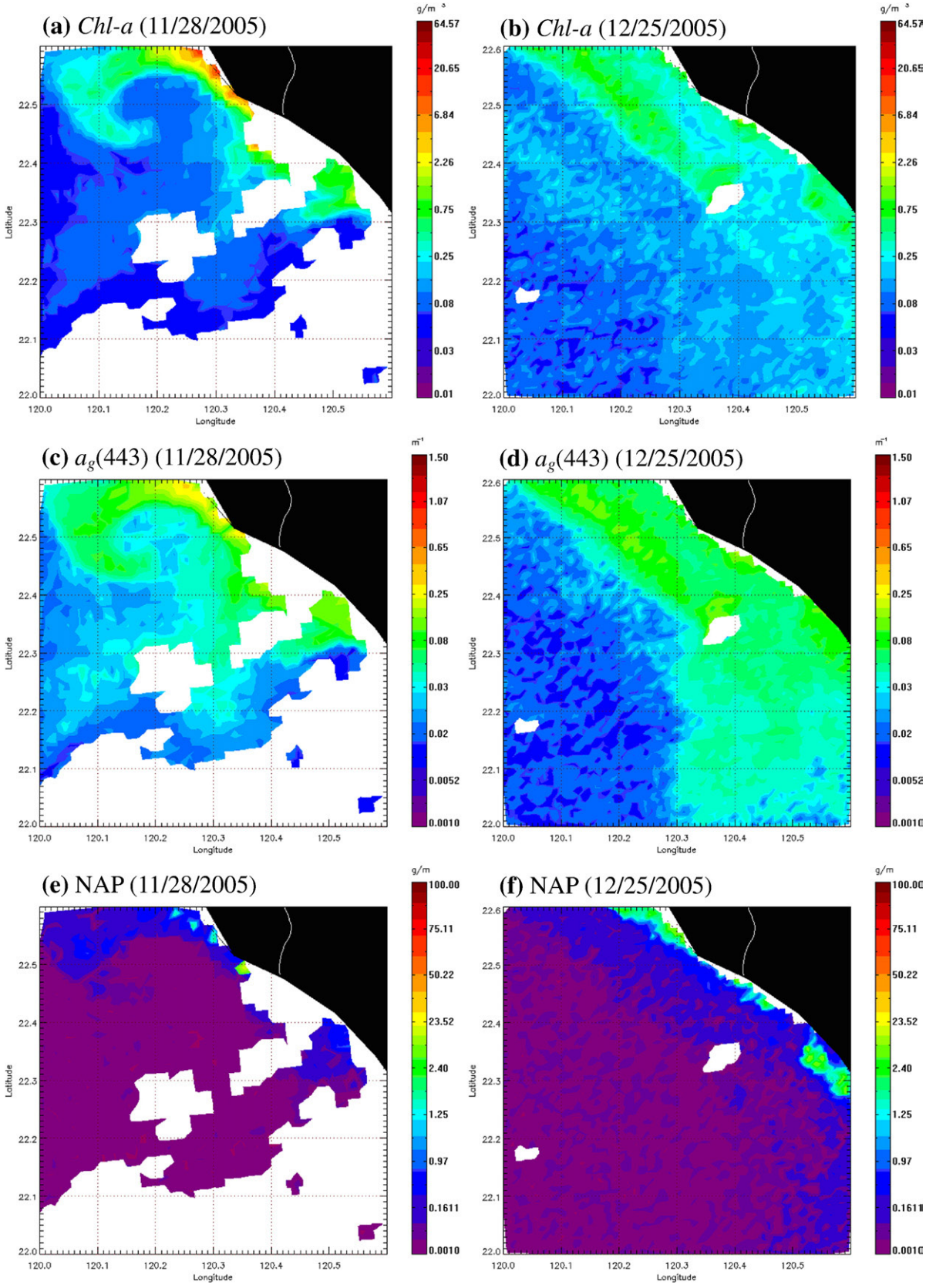

Fig. 11. Maps of *Chl-a*, a_g (443) and NAP derived from the MODIS-Aqua images that show the mesoscale eddy (11/28/2005) and the Kuroshio-dominated pattern (12/25/2005).

the fall (Fig. 2). Therefore, a very different dispersal pattern was observed on 10/6/2005 (Fig. 10). Although the original image is covered by clouds on the right-hand-side, a frontal pattern is evident. One possible mechanism of the front formation is the convergence between the southeastward transport and the intrusion of the Kuroshio Branch. On 11/14/2005 a small vortex can be identified on the maps of *Chl-a* and CDOM (Fig. 10). The small vortex might also evolve into a mesoscale eddy under appropriate conditions, as the example given in 11/28/2005 (Fig. 11). Finally, on 12/25/2005, the dispersal pattern is completely dominated by the Kuroshio Branch (Figs. 5 and 11) resulting in the discharge from the KPR being so low that there is no obvious point source.

4. Concluding remarks

The GA-SA approach is successfully employed to derive 12 maps of *Chl-a*, CDOM and NAP in the KPRSC region from MODIS-Aqua ocean color images in 2005. Taking into account different characteristics of *Chl-a*, CDOM and NAP, these maps are useful in studying the dispersal patterns in the KPRSC system. We categorized the surface dispersal patterns into coastal, northwestward and frontal patterns. We also have observed a sudden increase of biomass over a 2-day interval as well as a possible interaction between the river plume and the intrusion of the Kuroshio Branch. The major limitation of ocean color remote sensing is that the signal comes mainly from the sea surface. Nevertheless, the observed complex features are useful for model validation of the flow field in the KPRSC system.

Acknowledgements

The authors would like to thank the National Science Council of the Republic of China, Taiwan, for financial support under Contract Nos. NSC-95-2625-Z-006-004-MY3, NSC-95-2611-M-006-002, and the Landmark project under Contract Nos. B-023. to C.-C. Liu, and NSC-95-2611-M-006-013 to J. T. Liu.

References

Barale, V., Schlittenhardt, P.M. (Eds.), 1993. Ocean Colour: Theory and Applications in a Decade of CZCS Experience. Kluwer Academic, Dordrecht. 367 pp.

Chang, C.-H., Liu, C.-C., Wen, C.-G., 2007. Integrating semianalytical and genetic algorithms to retrieve the constituents of water bodies from remote sensing of ocean color. Optics Express 15 (2), 252–265.

Hooker, S.B., Esaias, W.E., Feldman, G.C., Gregg, W.W., McClain, C.R., 1992. An Overview of SeaWiFS and Ocean Color. NASA Tech. Memo, vol. 104566. NASA Goddard Space Flight Center, Greenbelt, Maryland, USA.

Huang, C.H., 2006. Development and application of the model of water quality and optical properties in reservoir. M.Sc. Thesis, National Cheng Kung University, Tainan, 232 pp.

Hung, J.-J., Hung, P.-Y., 2003. Carbon and nutrient dynamics in a hypertrophic lagoon in southwestern Taiwan. Journal of Marine Systems 42, 97–114.

Hung, J.-J., Yang, C.-Y., Lai, I.-J., 2004. Meterologic control on physical and chemical weathering rates and material fluxes from a tropical (Kaoping) river watershed in Taiwan. Joint AOGS 1st Annual Meeting and 2nd APHW Conference, Singapore, p. 759.

Lee, Z., 2003. Models, parameters, and approaches that used to generate wide range of absorption and backscattering spectra. IOCCG.

Lee, Z. (Ed.), 2006. Remote sensing of inherent optical properties: fundamentals, tests of algorithms, and applications. Reports of the International Ocean-Colour Coordinating Group, vol. 5. IOCCG, Dartmouth, Canada. 126 pp.

Lee, Z., Carder, K.L., Steward, R.G., Peacock, T.G., Davis, C.O., Patch, J.S., 1998. An empirical algorithm for light absorption by ocean water based on color. Journal of Geophysical Research 103 (C12), 27967–27978.

Liu, J.T., Lin, H.-L., 2004. Sediment dynamics in a submarine canyon: a case of river–sea interaction. Marine Geology 207 (1–4), 55–81.

Liu, J.T., Liu, K.J., Huang, J.C., 2002. The influence of a submarine canyon on river sediment dispersal and inner shelf sediment movements: a perspective from grain-size distributions. Marine Geology 181 (4), 357–386.

Liu, J.T., Lin, H.-L., Hung, J.-J., 2006. A submarine canyon conduit under typhoon conditions off Southern Taiwan. Deep Sea Research I 53, 223–240.

Milliman, J.D., Syvitski, J.P.M., 1992. Geomorphic/tectonic control of sediment discharge to the ocean: the importance of small mountainous rivers. Journal of Geology 100, 525–544.

Mitchell, B.G., Kahru, M., Wieland, J., Stramska, M., 2003. Determination of spectral absorption coefficients of particles, dissolved material and phytoplankton for discrete water samples. In: Mueller, J.L., Fargion, G.S., McClain, C.R. (Eds.), Ocean OPTICS Protocols for Satellite Ocean Color Sensor Validation. NASA, Maryland, pp. 39–60.

Mobley, C.D., 1999. Estimation of the remote-sensing reflectance from above-surface measurements. Applied Optics 38 (36), 7442–7455.

Toner, M., Kirwan Jr., A.D., Poje, A.C., Kantha, L.H., Muller-Karger, F.E., Jones, C.K.R.T., 2003. Chlorophyll dispersal by eddy–eddy interactions in the Gulf of Mexico. Journal of Geophysical Research 108 (C4), 3105. doi:10.1029/2002JC001499.

Welschmeyer, N.A., 1994. Fluorometric analysis of chlorophyll-a in the presence of chlorophyll-b and pheopigments. Limnology and Oceanography 39, 1985–1992.

Yung, S.M., 2006. Optical properties and distributions of dissolved organic matter in the Gaoping estuary and coastal zone. M.Sc. Thesis, National Sun Yat-Sen University, Kaohsiung, 91 pp.